Laser reflectometry of submegahertz liquid meniscus ringing

R. H. Farahi,[1,2,*] A. Passian,[1,2] Y. K. Jones,[3] L. Tetard,[1,2] A. L. Lereu,[1] and T. G. Thundat[1]

[1]*Oak Ridge National Laboratory, Oak Ridge, Tennessee 37831, USA*
[2]*Department of Physics, University of Tennessee, Knoxville, Tennessee 37996, USA*
[3]*Alcorn State University, Alcorn, Mississippi 39096, USA*
**Corresponding author: farahirh@ornl.gov*

Received July 23, 2009; revised August 17, 2009; accepted August 19, 2009;
posted September 4, 2009 (Doc. ID 114630); published October 8, 2009

Optical techniques that permit nondestructive probing of interfacial dynamics of various media are of key importance in numerous applications such as ellipsometry, mirage effect, and all-optical switching. Characterization of the various phases of microjet droplet formation yields important information for volume control, uniformity, velocity, and rate. The ringing of the meniscus and the associated relaxation time that occurs after droplet breakoff affect subsequent drop formation and is an indicator of the physical properties of the fluid. Using laser reflectometry, we present an analysis of the meniscus oscillations in an orifice of a piezoelectric microjet. © 2009 Optical Society of America

OCIS codes: 120.6650, 280.4788.

Given the broad range of applications using droplet formation by microjets, such as coating microelectromechanical system sensors, a better understanding of the physical processes associated with microjets is important. Wetsel modeled propagating capillary oscillations on the microjet column and optically determined instability growth rates [1]. Meinhart and Zhang used particle image velocimetry to visualize velocity fields and evolution of the meniscus inside translucent ink-jet printheads [2]. Yu *et al.* used the set level method for simulating viscoelastic ink ejection [3]. This Letter investigates meniscus oscillations through laser reflectometry. The meniscus "ringing" time, or relaxation time, has implications on the drop formation, unwanted satellite occurrences, and formation rates.

A single drop can be controllably formed by a transient pressure disturbance to the delivery channel from a piezoelectric transducer [4]. Continuous drops can also be formed from the breakup of liquid columns. A continuous stream of liquid jets from the orifice undergoes exponential capillary instabilities, $\delta(z)$, associated with surface tension, where z is the distance from the orifice. The growth of the instability eventually causes the jet to break at the length $L=(1/\gamma)\ln(R/\delta_0)$, where R is the radius of the column, δ_0 is the radial disturbance of the column from equilibrium at $z=0$, and γ is the deviatic growth parameter [1]. Consequently a drop is formed when the jet eventually succumbs to the instability at $\delta=R$. Upon break-off, the surface of the liquid in the orifice undergoes a transient oscillation for a period of time. This ringing is affected by the capillarity of the orifice-liquid interface as well as by the surface tension and viscosity of the liquid.

Meniscus measurements are difficult, because the position upstream inside the orifice is entirely undetectable except for transparent fluids in transparent devices where the meniscus in the orifice can be observed. We employed a dual optical measurement comprising laser reflectometry (LR) and jet-shadow detection, schematically shown in Fig. 1, that was able to analyze the meniscus as it recedes into the orifice with opaque liquids and/or opaque devices. Additionally, the static and dynamic longitudinal displacements of device piezoelectric elements as well as precise jet velocity were studied.

The test device is a tapered micropipette with a 30 μm diameter orifice that is bonded to a radially poled piezoelectric transducer tube. With a system trigger V_t at 500 Hz to 20 KHz, a pulsed waveform V_p on the transducer induces pressure waves in the micropipette to issue a droplet. The test fluid was isopropyl alcohol (IPA). The LR illumination and collection lenses, L1 and L2, are 12.7 mm FL plano-convex placed 20.5° with respect to the axis of the jet flow. After L1, the Gaussian beam spot size is calculated to be ~5 μm, an adequate spot size for probing a 30 μm orifice. Both the V_s=sum voltage and V_d=difference voltage of the LR position sensing detector (PSD) were monitored. For jet-shadow detection the photodiode detects the shadow cast when liquid interferes with the laser beam waist of ~50 μm. A reduction in

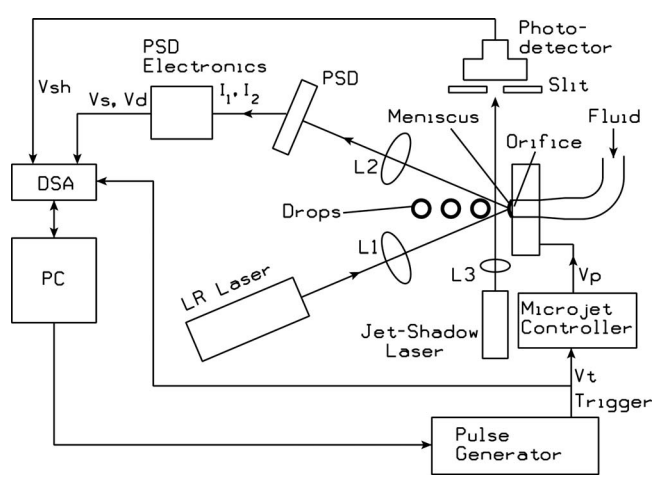

Fig. 1. Block diagram of experiment consisting of a microjet system, LR sensing, and jet-shadow detection.

 © 2009 Optical Society of America

the shadow voltage V_h is interpreted as liquid present in the laser beam. A digitizing signal analyzer (DSA) simultaneously recorded six transient signals: V_s, V_d, V_h, strobe, V_t, and V_p.

The meniscus is an evolving curved surface with a radius of curvature that changes with drop formation. To analyze the effects of curvature, the reflection of a finite collimated beam width of 5 μm from a meniscus having radius of curvature 23.4 μm in a 30 μm orifice is shown in Fig. 2, where the axis=L1 is incident at 21.5° to the jet axis Y and reflected at axis=L2. Large excursions of the meniscus result in extreme rays R1 and R2 not transmitted to the PSD, thus lowering the sum voltage and digressing from the meniscus displacement calibration.

A simplified analysis of the relationship between the meniscus position and displacement measured at the sensor is shown in Fig. 3. The meniscus shape is considered to be determined by a sphere that passes through the circle that defines the orifice. The meniscus position is defined by the segment C_0M or y_m. This assumption is reasonable as long as the meniscus is less than the diameter of the orifice, d. The radius of curvature of the meniscus is related to y_m by $R_m = y_m/2 + d^2/(8y_m)$. The incident beam is reflected with respect to the normal to the surface, which is n_0, n_+, and n_- for a flush, convex, and concave meniscus, respectively. For a positive meniscus the beam hits C_+ and reflects with respect to the local normal n_+, defined by the segment O_+C_+, to hit the sensor at S_+. The PSD measures the displacement between S_0, or zero position, and S_+. A similar situation is obtained for a negative meniscus position.

The beam displacement u from S_0 can be determined as a function of y_m. The coordinates that define the point where the incident beam hits the meniscus are $(-x_c, y_c)$ at C_+ when y_m is positive and $(x_c, -y_c)$ at C_- when y_m is negative are described with a second-degree polynomial $x_c = b + (b^2 - 4ac)^{1/2}$ and $y_c = x_c \cot \alpha$, where the coefficients are $a = \cot \alpha^2$, $b = -2(R_m - y_m)\cot \alpha$, and $c = y_m^2 - 2R_m y_m$. The angle α_r that the reflected beam forms with the y axis is $\alpha_r = \alpha - 2 \arctan[x_c/(R_m - y_m + y_c)]$. The point (x_s, y_s) where the reflected beam hits the sensor for positive y_m is $x_s = (d_s \sec \alpha - y_c - x_c \cot \alpha_r)/(\tan \alpha + \cot \alpha_r)$ and $y_s = -x_s \tan \alpha + d_s \sec \alpha$, where d_s is the segment C_0S_0, the distance between a flush meniscus and the sensor. The coordinates where the beam hits on the sensor when the meniscus is undeformed ($y_m = 0$) are $x_0 = d_s \sin \alpha$ and $y_0 = d_s \cos \alpha$. The displacement u_a of the beam on the sensor as measured from S_0 for positive y_m is $u_a = [(x_s - x_0)^2 + (y_s - y_0)^2]^{1/2}$. The displacement of the beam for a negative y_m is calculated similarly using $(x_c, -y_c)$. From the above equations, the displacement u of the beam on the sensor from $-d/2 \leq y_m \leq d/2$ is plotted in the inset of Fig. 3 for $d = 30$ μm, $d_s = 20$ mm, and $\alpha = 69.5°$.

The results are shown in Figs. 4 and 5, where the LR signal uses the y axis. For correlation, CCD camera images are noted at various strobe times to identify drop formation and visually discernible meniscus displacements, as demarked by eight dotted lines.

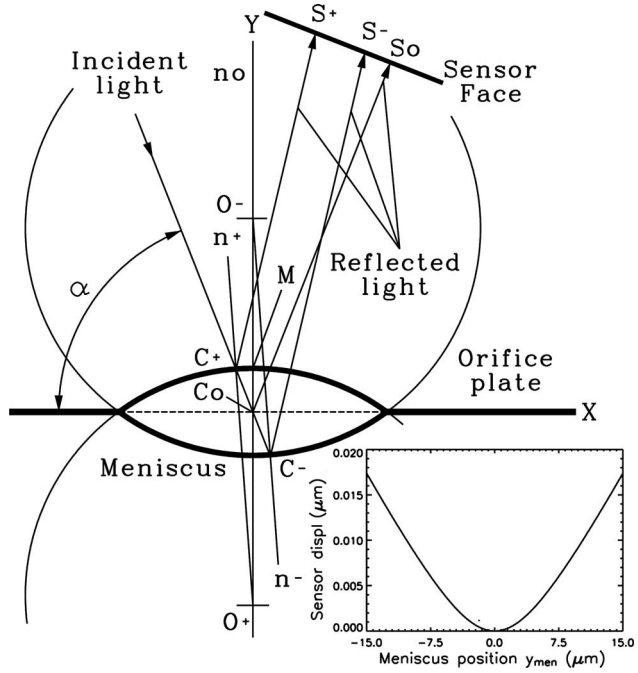

Fig. 3. Geometrical relationship between the reflected probe light at the sensor face (S) and the position of the meniscus (M). The inset is a plot of $(S_0 - S)$ versus M.

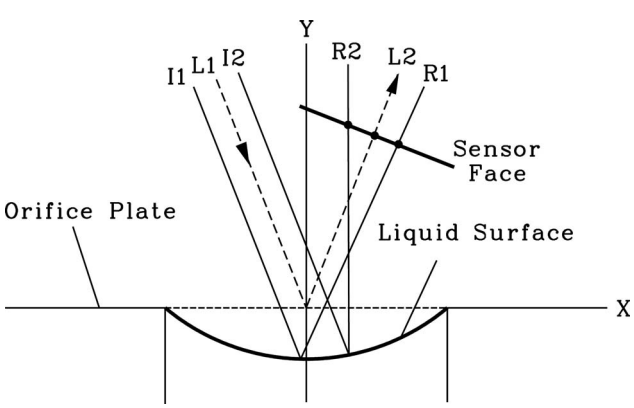

Fig. 2. The effect of meniscus curvature and beam width on the LR sensor signal. The angular deflection of the extreme rays of reflected beam, R1 and R2, result in the loss of collimation on the sensor plate.

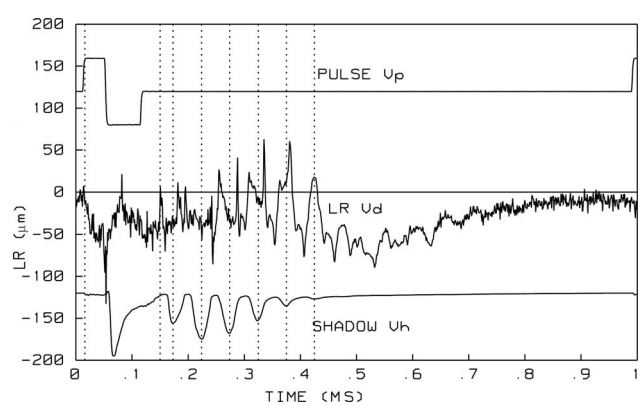

Fig. 4. Transient recordings of liquid surface motion. The LR signal is calibrated in micrometers (y axis). The overlaid jet-shadow signal and excitation waveform are plotted in arbitrary units.

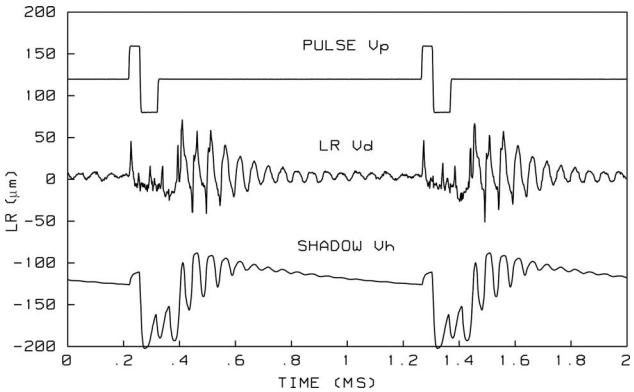

Fig. 5. Transient recordings of meniscus motion where the device surface is wetted.

During the positive part of the pulse, the meniscus recessed downstream about 45 μm (location 1 from the left). During the negative part of the pulse a long tail is being formed until it finally breaks off at 0.42 ms; the jet-shadow signal reduces significantly, and the LR signal is out of range. After break-off (location 2) the meniscus begins to oscillate at ~200 KHz in progressively smaller excursions for about 0.3 ms according to the CCD camera; the jet-shadow signal minimas correspond (locations 3–8). The oscillation frequency is on the order of the speed of sound through the 3 mm device tubing. The LR signal is following the oscillations with a waveform shape consistent with Fig. 3. After the last oscillation is identified by the CCD camera and the jet-shadow signal (location 8), the LR signal continues to track the meniscus oscillations for another 0.4 ms, which are now too small to be detected by the other two methods. In Fig. 5(a) a wetted surface area around the orifice occurred, causing a very low radius of curvature that produced a relatively smooth LR signal.

Jet-shadow measurements of drop velocity triggered at 2.5 KHz were taken at 110 μm and 310 μm downstream from the orifice where drop formation occurs. The distance between the two measurements was $\Delta z = 200$ μm, and the time between minimas in the shadow voltage was $\Delta t = 0.1152$ ms, resulting in a drop velocity $U_d = \Delta z / \Delta t = 1.74$ m/s. The jet velocity $U = f\lambda$ is related to the disturbance wavelength λ of the column and drop frequency $f = \omega / 2\pi$. The drop velocity and jet velocity are related by $U_d = U[1 - (2T/\rho R)/U^2]$, where T and ρ are fluid parameters surface tension and density, respectively [1]. For this device, 1 to 10 m/s are typical velocities.

Transient measurements of the device motion were taken by applying a pulse (0.4 Hz at 60% duty cycle with 50 V amplitude) to a dry device. Shown in Fig. 6, longitudinal displacements up to 1 μm may occur from the device itself. Ringing occurs for almost 2 ms at ~6 KHz and is expected to dampen when filled with liquid. The transient displacement is consistent

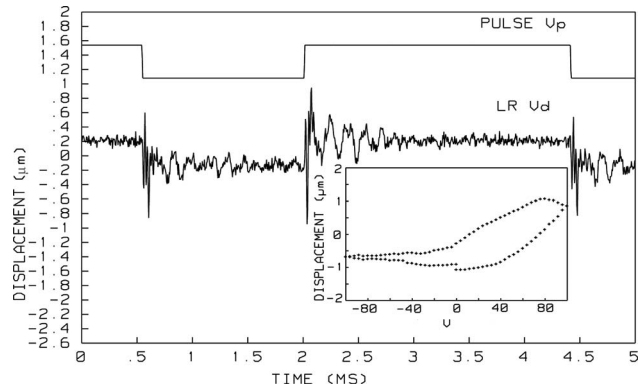

Fig. 6. Dynamic longitudinal displacement of piezoelectric element in microjet device. The inset is the static longitudinal displacement of piezoelectric actuator, revealing hysteresis.

with the static measurement. A static measurement was taken by applying a ramped voltage on the device from 0 V to 100 V to −100 V, and back to 0 V, plotted in the inset of Fig. 6. The longitudinal displacement was about 8 nm/V for the increasing voltage ramp, corresponding to the theoretical displacement provided by the manufacturer. In the returning decreasing voltage, hysteresis was observed and expected.

In a continuation of our studies in digital microfluidics [5–7], an analysis of meniscus oscillations in a microjet device has been presented using laser reflectometry. Meniscus movements, jet velocity, and displacements due to the device piezoelectric elements were analyzed. Our optical approach may be used to measure surface movement of many types of opaque/translucent liquids, including inks, polymers, and bioactive molecules.

This research was supported by the Department of Homeland Security-sponsored Southeast Region Research Initiative (SERRI) at the Department of Energy's Oak Ridge National Laboratory (ORNL). Oak Ridge National Laboratory, Oak Ridge, Tennessee, 37831-6123, is managed by UT-Battelle, LLC for the Department of Energy under contract number DE-AC05-0096OR22725.

References

1. G. C. Wetsel, Jr., J. Appl. Phys. **51**, 3586 (1980).
2. C. D. Meinhart and H. Zhang, J. Microelectromech. Syst. **9**, 67 (2000).
3. J.-D. Yu, S. Sakai, J. A. Sethian, C. D. Meinhart, and H. Zhang, J. Comput. Phys. **220**, 568 (2007).
4. B. Wallace, AMD (Am. Soc. Mech. Eng.) **4**, 1 (1989).
5. R. H. Farahi, A. Passian, T. L. Ferrell, and T. Thundat, Appl. Phys. Lett. **85**, 4237 (2004).
6. R. H. Farahi, A. Passian, T. L. Ferrell, and T. Thundat, Opt. Lett. **30**, 616 (2005).
7. A. Passian, S. Zahrai, A. L. Lereu, R. H. Farahi, T. L. Ferrell, and T. Thundat, Phys. Rev. E **73**, 066311 (2006).